AIAA JOURNAL
Vol. 33, No. 10, October 1995

Measurements of Supersonic Wing Tip Vortices

Michael K. Smart,* Iraj M. Kalkhoran,† and James Bentson‡
Polytechnic University, Brooklyn, New York 11201

An experimental study of supersonic wing tip vortices has been conducted at Mach 2.49 using small-scale four-hole and five-hole conical probes. The study was performed 2.25 chords downstream of a semispan rectangular wing at angles of attack of 5.7 and 10.4 deg. The main objective of the experiments was to determine the Mach number, flow angularity, and total pressure distribution in the core region of supersonic wing tip vortices. A secondary aim was to demonstrate the feasibility of calibrating a conical probe using a computational solution to predict the flow characteristics. Results of the present investigation showed that the numerically generated calibration data can be used for pointed nose four-hole conical probes but were not sufficiently accurate for conventional five-hole probes due to nose bluntness effects. A combination of four-hole conical probe measurements with independent pitot pressure measurements indicated a significant Mach number and total pressure deficit in the core regions of supersonic wing tip vortices, combined with an asymmetric "Burger-like" swirl distribution.

Nomenclature

C_p	= pressure coefficient
$C_{p\eta}$	= pressure coefficient difference, $(P_d - P_b)/q$
$C_{p\xi}$	= pressure coefficient difference, $(P_a - P_c)/q$
D_s	= core diameter of strong vortex
D_w	= core diameter of weak vortex
M	= Mach number
N	= conical probe nose diameter
P	= pressure
q	= dynamic pressure
x, y, z	= Cartesian coordinates
α	= vortex generator angle of attack
β	= circumferential angle (Fig. 3)
δ	= pressure tap distance from probe tip
θ	= pitch angle
ν	= uncertainty
τ	= magnitude of swirl angle, $\tan^{-1}\lvert M_x/M_z\rvert$
ϕ	= roll angle
χ	= distance from probe tip

Subscripts

a, b, c, d, e	= conical probe pressure tap labels (Fig. 2)
av	= average
c	= cone surface
s	= static
x, y, z	= Cartesian coordinates
0	= settling chamber
1	= total
2	= pitot
∞	= freestream

Introduction

MANY fluid flow problems in aerodynamics and engineering are dominated by vortical structures. These vortical structures, commonly called vortices, are the result of the separation and subsequent roll-up of boundary layers that have been forced to leave solid surfaces. Of particular interest to aerodynamicists are the vortices generated by the lifting surfaces of an aircraft. For example, vortices produced at the wing tips of an aircraft are an integral part of the generation of lift, and an understanding of their structure is important from a general performance standpoint. Also, the vortices generated by the forebody or canards of an aircraft flying at angle of attack can interact with downstream aerodynamic surfaces or be ingested by engine intakes, causing stability and control or engine blockage problems during particular flight maneuvers. In an effort to expand the experimental database for supersonic vortex flows, various fundamental vortical interaction studies have been initiated.[1-3] These studies have primarily been concerned with the interaction of supersonic wing tip vortices with lifting surfaces and shock fronts. To thoroughly analyze the results of these experiments, a parallel program has been undertaken to develop the capability for measurement of the Mach number, total pressure, and flow angularity of the incoming wing tip vortices.

Incompressible wing tip vortices have been extensively studied over many years. McCormick et al.[4] examined the decay of tip vortices with downstream distance in flight experiments. Near-field characteristics of tip vortices were measured in a wind tunnel by Orloff[5] and Corsiglia et al.[6] and in a water tank by Baker et al.[7] In general, low-speed wing tip vortices have been found to exhibit tangential velocity distributions similar to a Burgers vortex, in combination with a wake-like streamwise velocity distribution. Some asymmetry of the tangential velocity is typically observed,[5] and the streamwise velocity deficit in the vortex core is attributed to the momentum deficit in the boundary layer on the wing. Conversely, information concerning supersonic wing tip vortices is very scarce in the open literature. Experimental work has been performed by Davis[8] and Adamson and Boatright[9] examining the flow structure behind rectangular wings at supersonic speeds. These studies were aimed at determining the wash characteristics of the wake, and little information was reported on the characteristics of wing tip vortices. Pitot surveys of supersonic wing tip vortices were reported by Wang and Sforza[10] indicating significant pitot pressure deficits relative to the freestream. To the authors' knowledge, the current investigation is the first attempt to measure the detailed flow structure in the core region of supersonic wing tip vortices.

Multihole conical probes have traditionally been the instrument of choice for measurements in three-dimensional supersonic flowfields. Pioneering work by Centolanzi,[11] using a 20-deg half-angle conical probe with a base diameter of 9.5 mm, showed that five-hole conical probes could be used to obtain accurate simultaneous measurements of Mach number, total pressure, and flow angularity in supersonic flows. The method he reported involved the experimental calibration of a five-hole probe at numerous pitch and roll angles over a range of Mach numbers. These data were then cleverly cast into calibration curves so that the Mach number, total pressure,

Presented as Paper 94-2576 at the AIAA 18th Aerospace Ground Testing Conference, Colorado Springs, CO, June 20–23, 1994; received July 7, 1994; revision received Jan. 6, 1995; accepted for publication Feb. 1, 1995.

*Graduate Research Fellow, Department of Aerospace Engineering. Student Member AIAA.
†Assistant Professor, Department of Aerospace Engineering. Member AIAA.
‡Industry Professor, Department of Aerospace Engineering.

and flow angularity could be obtained directly from the cone surface pressure measurements using an iterative procedure. This technique has become the standard, and numerous investigators[12,13] have reported successful calibration and use of their own conical probes with diameters as small as 1.1 mm.

The drawbacks of conventional conical probes are their relatively slow response time, on the order of 1 s, and the time-consuming experimental calibration procedure. In an attempt to circumvent difficulties associated with slow response time, Naughton et al.[13] reported the use of a miniature five-hole probe incorporating fast response piezoelectric pressure transducers inside the wind tunnel. This probe had a 30-deg half-angle, a diameter of 1.1 mm and was calibrated in the Mach number range of 2–4. Their results indicated an improvement in response time of two orders of magnitude over conventional probes, and they used the probe to successfully measure supersonic streamwise vortices generated by swirl vanes with a core diameter of approximately 4 mm. Another difficulty with the use of conventional conical probes is the tedious experimental calibration procedure. To emphasize this point, a typical calibration of a five-hole conical probe is summarized here. For a chosen Mach number, the probe is placed at a specified pitch angle and then rotated about its axis in small increments, collecting the pitot pressure and the four surface pressures at each roll angle. This process is repeated at different pitch angles up to the desired maximum and at a few Mach numbers in the range of interest. For typical roll increments of 10 deg, with 5 different pitch angles and 3 Mach numbers, this amounts to 525 sets of data. This procedure must be performed for each probe of different geometry, and some cursory checking of the calibration should be performed for each similarly shaped probe that is fabricated. It is clear that the amount of wind-tunnel time needed to complete this process is prohibitive for many practical applications.

An alternative to experimental calibration is the generation of probe calibration data using computational solvers. In recent years computational fluid dynamics has advanced to the point where the accurate prediction of supersonic flow past smooth pointed bodies at moderate angles of attack is possible. An example of this is reported in Refs. 14 and 15, where a computational solution of the parabolized Navier–Stokes equations was shown to accurately predict Mach 8 force and moment data for a 10-deg half-angle conical body at angles of attack up to 20 deg. With particular application to conical probes, it is expected that the supersonic flow past a pitched conical probe with moderate nose bluntness can readily be solved using currently available numerical techniques. Furthermore, it is expected that for conical probes that have the static pressure taps located a large distance from the nose (large δ/N), the flow can be adequately predicted using a solution of the conical equations.[16] If this is not the case, a full three-dimensional solution is needed requiring a significant increase in computational time. The use of numerical solutions to calibrate conical probes is clearly a viable alternative to experiment. Satisfactory numerical calibration of probes with large δ/N will require the least amount of computational effort. Calibration of conical probes with pressure taps close to the nose (small δ/N) will be the most difficult to accomplish due to the effect of nose bluntness.

The main objective of this investigation was to determine the Mach number, total pressure, and swirl distributions in the core region of supersonic wing tip vortices. To accomplish this task, both a four-hole and a five-hole conical probe were commercially acquired. A cone half-angle of 30 deg was chosen for both probes, and each had a diameter of 3.2 mm, which was the smallest available size. The calibration curves used for the conical probes were generated using computational solutions instead of the conventional experimental calibration. Conical probe surveys of the tip vortices generated by a rectangular half-wing at $\alpha = 5.7$ and 10.4 deg are presented in this paper. The results of these surveys add to the scarce amount of experimental information on supersonic wing tip vortices currently available in the literature. Such data are important for the increased understanding of supersonic vortical flows and for use as input to numerical computations. A discussion of the use of numerically generated calibration curves is also included in this paper due to the original nature of this approach.

Experimental Program

Wind Tunnel and Test Conditions

The current investigation was conducted in Polytechnic University's supersonic blowdown wind-tunnel facility.[17] This is an intermittent blowdown wind tunnel with a square test section of 381 × 381 mm and is capable of producing unit Reynolds numbers in the range of 2.6×10^7 to 2.2×10^8 per meter over a Mach number range from 1.75 to 4.0. The experimental study reported here was conducted at a nominal test section Mach number of 2.49. The stagnation pressure and temperature for these experiments were 0.45 MPa and 290 K, respectively, resulting in a unit Reynolds number of 4.5×10^7 per meter. A typical test time for the experiments was 3 s.

Experimental Arrangement

A schematic of the experimental arrangement is shown in Fig. 1a, along with a dimensioned drawing in Fig. 1b. The vortex generator used in the experiments was a rectangular half-wing with diamond-shaped cross sections (8 deg half-angle), a chord length of 50 mm, and a span of 163 mm. It was mounted vertically at the base of the test section with angles of attack of 5.7 and 10.4 deg. For structural stability, the conical probes were mounted in a 25-mm-diam tube that protruded vertically through the test section ceiling (Fig. 1). The probes were situated with their tip approximately 113 mm (2.25 vortex generator chords) downstream of the half-wing trailing edge and were able to be traversed in the vertical direction in increments as small as 0.8 mm. A wedge-shaped fin (18 deg included angle) was installed with its leading edge 13 mm behind the probe tip to isolate the conical probes from any upstream influence of the support tube bow shock (Fig. 1).

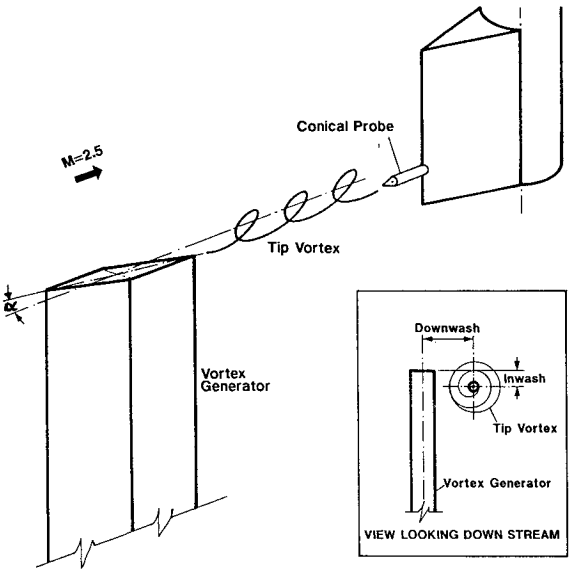

Fig. 1a Schematic of experimental arrangement.

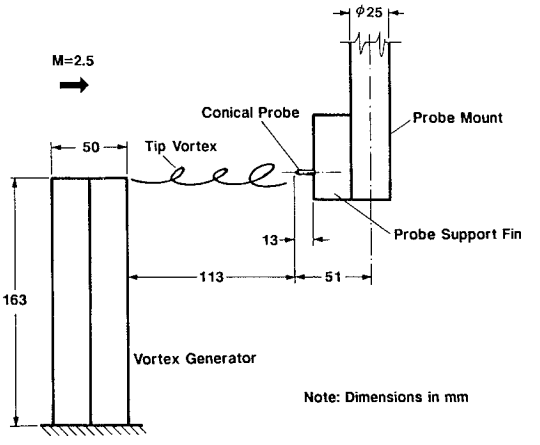

Fig. 1b Dimensioned drawing of experimental arrangement.

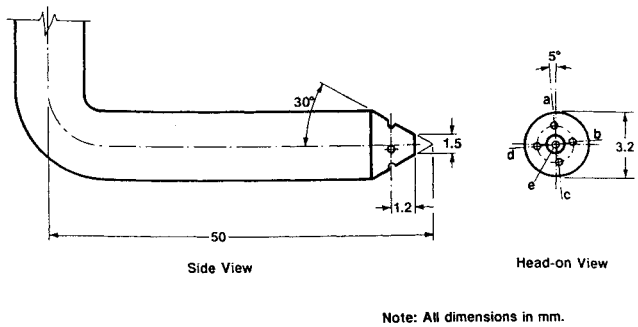

a) 5-hole probe

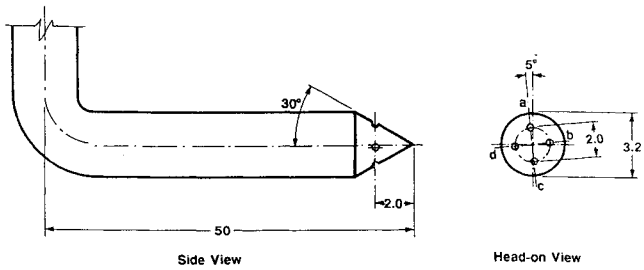

b) 4-hole probe

Fig. 2 Conical probes.

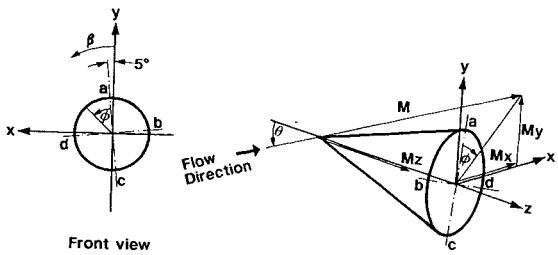

Fig. 3 Spherical coordinate system.

Conical Probes

Two small-scale conical probes were used in the study, dimensioned drawings of which are shown in Fig. 2. Each probe had a diameter of 3.2 mm and a half-angle of 30 deg. The five-hole conical probe included four equally spaced static pressure taps flush with the cone surface (denoted a, b, c, and d) a distance $\delta = 1.2$ mm from the probe tip and a total pressure tapping (denoted e) placed centrally on a blunted nose of diameter $N = 1.5$ mm ($\delta/N = 0.8$). The four-hole conical probe included four equally spaced static pressure taps on the cone surface a distance $\delta = 2.0$ mm from the probe tip and a nose bluntness ratio of $\delta/N = 7.1$. The diametral distance between opposite surface pressure taps on both probes was 2 mm. The probes were constructed with a 90-deg elbow 50 mm behind the tip to reduce the line length between the pressure taps and the transducers to 360 mm. The pressure lines in the probe tips had an internal diameter of 0.4 mm. A line length of 360 mm at this diameter was expected to degrade probe response time to an unacceptable level for typical test times of 3 s. To circumvent this problem, the internal diameter of the pressure lines was increased to 0.6 mm after the elbow. Benchtop tests indicated that the time response of the conical probes to rapid pressure changes on the order of 1 atm was approximately 0.5 s.

The spherical coordinate system shown in Fig. 3 was used for the study. The z direction was parallel with the freestream and the probe axis, whereas the x and y directions were horizontal and vertical, respectively (lateral and spanwise with respect to the half-wing). The conical probes were manufactured with the static pressure taps a, b, c, and d at circumferential angles $\beta = 5, 275, 185$, and 95 deg, respectively. The sign conventions for the pitch angle θ and the roll angle ϕ of the probes were as shown in Fig. 3. Given that M, θ, and ϕ are known, the Mach number components were calculated as follows:

$$M_x = -M \sin\theta \sin\phi$$

$$M_y = -M \sin\theta \cos\phi$$

$$M_z = M \cos\theta$$

Table 1 Uncertainty estimates

Flow property	Freestream, $M = 2.49$, $\theta = 10$ deg	$\alpha = 5.7$ deg, 0.8 mm below axis
M	2.489 ± 0.068 (±2.7%)	1.98 ± 0.064 (±3.2%)
P_1, kPa	439.2 ± 22.4 kPa (± 5.1%)	161.2 ± 7.0 kPa (±4.3%)
P_s, kPa	26.45 ± 1.25 kPa (±4.8%)	21.23 ± 1.29 kPa (±6.1%)
M_x	0.448 ± 0.017	−0.292 ± .014
M_y	0.002 ± 0.006	0.173 ± 0.016
M_z	2.448 ± 0.067	1.952 ± 0.064

Instrumentation and Data Acquisition System

Five Kulite pressure transducers (model ITQ-1000) were used in the experiments. The transducers used for cone surface pressure measurement had a useful range from 0–136 kPa, whereas the transducer used to measure pitot pressure had a useful range from 0–345 kPa. All transducers had a natural frequency response of 12 KHz. Output from the transducers was first amplified by Honeywell Accudata 122 dc amplifiers and then digitized using a Metrabyte Das-16F, 12-bit analog-to-digital converter board at a rate of 500 Hz per channel for a period of 3 s. Shadowgraphs were taken of the flowfield using a spark light source that provided microsecond range exposure times. A simple laser-based light sheet technique was also used for planar visualization of the flowfield.

Uncertainty Estimates of Flow Properties

The experimental errors associated with typical cone surface and pitot pressure measurements reported in this paper were $v_c = \pm 0.68$ kPa and $v_2 = \pm 1.70$ kPa, respectively. Typical values and uncertainty estimates for the flow properties calculated using these pressure measurements are listed in Table 1. The values of and uncertainties in the Mach number M, the total pressure P_1, the static pressure P_s, and the Mach number components M_x, M_y, and M_z are presented for both a typical freestream conical probe measurement and a typical measurement in the core region of a supersonic wing tip vortex. The uncertainty estimates listed in Table 1 are representative of all measurements performed for the work.

Computational Calibration of Conical Probes

As described earlier, the calibration of conical probes has traditionally required an exhaustive amount of experimental data taken with the probe at different pitch and roll angles, over a range of Mach numbers. In the present study the conical probe calibration curves were generated using a computational solution. These solutions were obtained using a conical Navier–Stokes solver developed by Marconi.[18] This code uses a computational algorithm based on Beam and Warming's approximate factorization[19] in conjunction with Roe's flux difference splitting.[20] The solution of the equations is accomplished using an upwind alternate direction implicit technique similar to that of Thomas and Walters.[21]

The supersonic flow past circular cones at angle of attack has been extensively studied both experimentally and computationally.[16,22,23] It is generally known that for relative incidences (pitch angle/cone half-angle) up to 2.5, the viscous/inviscid flowfield maintains both a symmetric and nearly conical nature as long as the flow remains laminar or is essentially turbulent from the apex. Conical Navier–Stokes solvers such as the one described earlier have been successful in adequately predicting these flows.[16] Also, at relative incidences less than unity, Reynolds number effects have been found to be negligible.[23] The Reynolds number in the current study, using $\delta = 2$ mm as the relevant length scale, was found to vary from 2×10^4 in the vortex cores to 9×10^4 in the freestream. The flow over the cone probe is therefore expected to be laminar for all measurements. The maximum pitch angle of the current study was 25 deg, which corresponds to a relative incidence of 0.83; hence Reynolds number

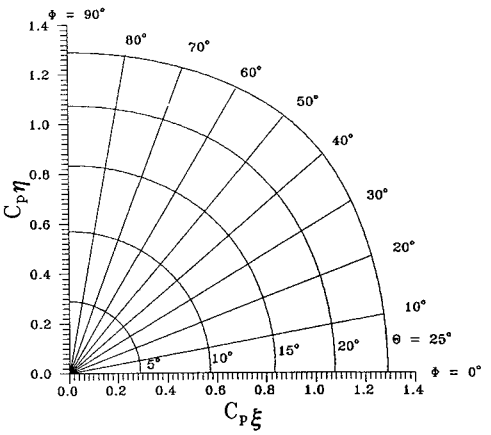

Fig. 4 Numerically generated calibration chart for $M = 2.5$.

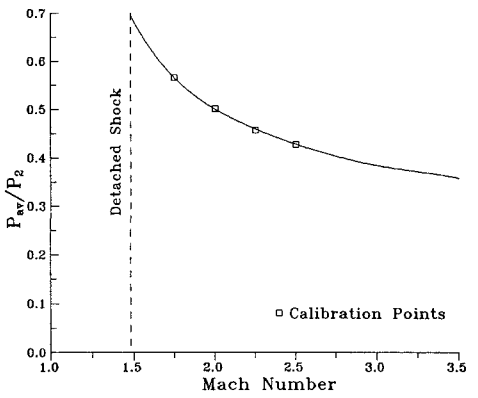

Fig. 5 Variation of average cone pressure with Mach number.

effects are expected to be negligible. In light of these factors, conical Navier–Stokes solutions were compared with results generated by running the code as an Euler solver. Good agreement between the viscous and inviscid calculations was found for the cases of interest. It was decided that the extra computational time required for the Navier–Stokes solutions was not justified; hence all numerical data presented in this work were obtained from inviscid computations.

The process of numerically generating a full set of calibration curves for a conical probe with specified half-angle is as follows. First, a conical grid is generated to match the probe geometry and the expected flowfield. For the current work the 81 × 63 grid was sheared to the leeward side to capture all shocks. Computational solutions are then obtained for each combination of Mach number and pitch angle in the range of interest. Note that each run calculates the complete flow past the probe, so that the full circumferential pressure distribution can be extracted from a single run, thereby eliminating the need to specify a roll angle. The 525 sets of data required for the typical experimental calibration described earlier can be obtained with 15 computational runs. For the current work the Mach number range of interest was between 1.75 and 2.5, and the maximum cone pitch angle was 25 deg. These values represent the anticipated Mach numbers and maximum flow angularity in the core region of supersonic wing tip vortices. Calibration curves were generated for $M_\infty = 1.75$, 2.0, 2.25, and 2.5 at pitch angles between 0 and 25 deg in increments of 5 deg (24 runs). A typical calibration curve for Mach 2.5 is shown in Fig. 4. After Centolanzi,[11] the surface pressure data at each θ and ϕ are plotted vs $C_{p\eta} = (P_d - P_b)/q$ and $C_{p\xi} = (P_a - P_c)/q$. Previous investigators[11,13] found that little variation with Mach number occurs when experimental probe data are plotted in this form. The numerical solutions generated for the current work also follow this trend.

The iterative procedure for determining the Mach number, total pressure, and flow angularity from the measured pitot and surface pressures is fully described in Refs. 11 and 13. In short, the flow Mach number is initially estimated from the ratio P_{av}/P_2 assuming that $\theta = 0$ deg. Figure 5 shows a plot of $P_{av}/P_2(\theta = 0 \text{ deg})$ vs Mach number obtained from the present computations. Next, the coefficients $C_{p\xi}$ and $C_{p\eta}$ are calculated. The two Euler angles, ϕ and θ, can then be determined from calibration maps such as Fig. 4. In general, iteration is required because P_{av}/P_2 varies with θ. Hence, after a first estimate of Mach number and flow angularity has been made, the Mach number must be adjusted for this variation and the process repeated. It has been found[11,13] that for five-hole conical probes a maximum of four iterations are typically required. In summary, the determination of flow properties using the numerically generated calibration curves is identical to the conventional procedure, except that the calibration data are collected by computation rather than experiment.

Experimental Results and Discussion

Conical Probe Operation

The initial phase of the experimental program was concerned with establishing the accuracy, repeatability, and time response characteristics of the conical probe measurements. Figure 6 shows the normalized pressure vs time traces obtained using the four-hole probe with test section Mach number of 2.49 and $\theta = 20$ deg. The pressures recorded for all tappings are observed to reach a steady-state value after approximately 0.75 s. This result is typical of both the four-hole and five-hole probes, indicating that the time response of the probes is acceptable for use in short duration blowdown wind tunnels. In general, the initial 1 s of a typical 3-s run was discarded during data processing, and the remainder of the data were time averaged to obtain mean values of the surface pressures. Some small-amplitude unsteadiness was observed in conical probe measurements near the axes of the vortices. This is thought to be caused by the random wandering of the vortices known as vortex meander, a phenomenon also observed in low-speed wing tip vortices[7] and believed to be due to freestream turbulence. An attempt to visualize the amplitude of any vortex meander that occurs in the current experiments was performed using spark shadowgraph images of the tip vortices taken at a rate of two per second. These showed no discernable vortex meander, indicating that any vortex meander that may occur in the current experiments is of small amplitude.

Satisfactory use of the four-hole and five-hole conical probes depends entirely on the accuracy with which the numerical solution predicts their surface pressure distribution. A comparison between the numerical and experimental results at Mach 2.49 is shown in Fig. 7, with the probes at $\theta = 0$, 5, 10, 15, and 20 deg. It can be seen that, except for a slight underprediction of the peak pressure on the windward side of the probe ($\beta = 90$ deg), the numerical scheme predicts the four-hole conical probe surface pressure with high accuracy. These comparisons indicate both the good accuracy with which the computations are able to calculate the surface pressure distribution on a cone, as well as the small tolerances within which the four-hole probe was constructed. The surface pressures measured on the five-hole probe, however, differed from both the four-hole probe and numerical results, particularly on the leeward side ($\beta = 270$ deg) where a significantly greater suction was observed.

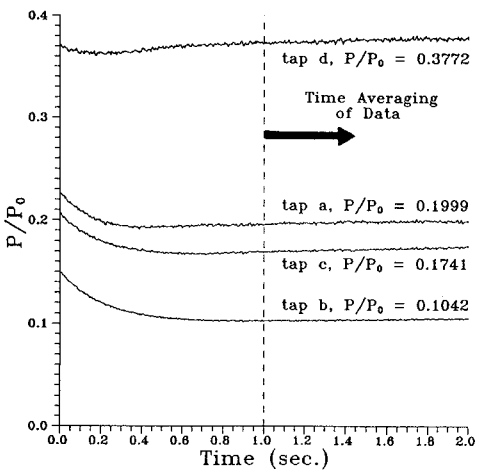

Fig. 6 Time history of cone surface pressures, $M = 2.49$, $\theta = 20$ deg.

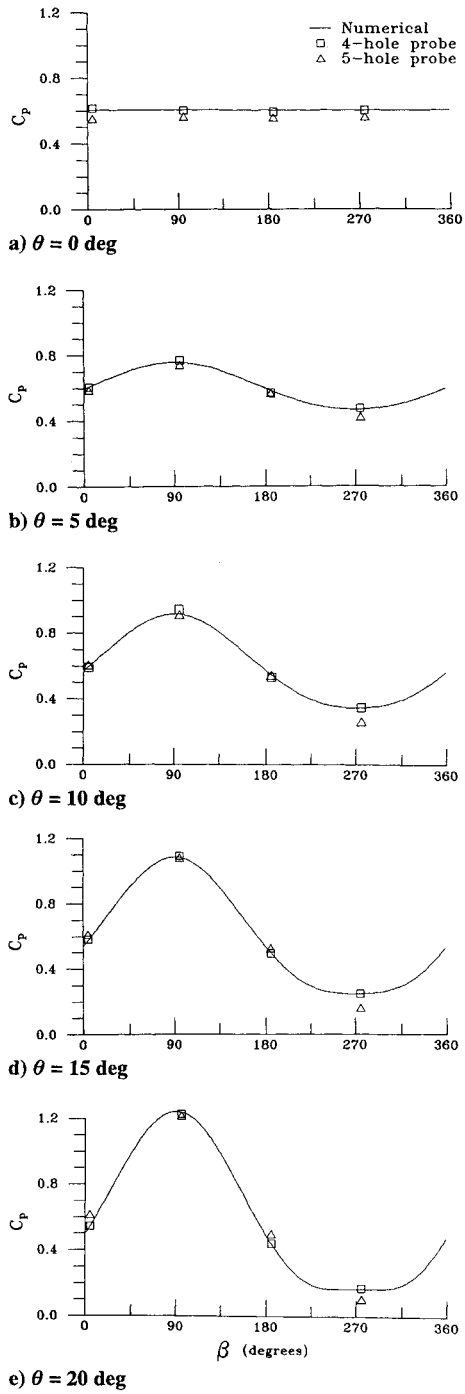

Fig. 7 Circumferential cone surface pressure coefficient distribution at M= 2.49.

The generally lower surface pressures observed for the five-hole probe at small pitch angles are consistent with those reported in the literature where a blunted nose has been found to cause an overexpansion in the region local to the nose, followed by an asymptotic approach to the pointed cone results. Krasnov[24] supplied a universal curve for predicting the scale of the overexpanded region on blunted cones at zero angle of attack. For flat nosed cones with 30-deg half-angle at Mach 2.5, this curve predicts that the pressure coefficient on the cone surface approaches 99% of the pointed cone result at $\chi/N = 3.22$ (where χ is the downstream distance measured from the flat nose). The pressure taps on the five-hole probe used in this study are at $\chi/N = 0.80$, which is well within the region expected to be affected by nose bluntness. The effect of nose bluntness on cones at angle of attack is not as easy to quantify, but it is hardly surprising that the five-hole probe shows significant overexpansion due to its blunt nose, particularly on the leeward side. The pressure taps on the four-hole probe are at $\chi/N = 7.1$, well outside the region affected by the nose. Based on the results shown in Fig. 7, it is expected that calibration curves generated by the conical Euler solver can be used with confidence for the four-hole conical probe. However, satisfactory numerical calibration of the blunted five-hole probe used here would require a fully three-dimensional numerical scheme and a significant increase in computational time and effort.

The restriction of numerical calibration to the four-hole conical probe introduces an additional complexity to the determination of the flow properties. That is, the pitot pressure must be measured independent of the cone surface pressures. To fully determine the properties at a point, two measurements are required: a four-hole probe measurement (supplying the cone surfaces pressures) and a separate five-hole probe measurement to supply the pitot pressure. This means that data must be combined from two separate wind-tunnel runs, requiring a good degree of repeatability between runs. In light of this requirement, considerable repetition of runs was performed in the current study. It was found that the time-averaged pitot and surface pressure measurements exhibited good repeatability (within 2%) for identical flow conditions. Limitation of numerical calibration to the four-hole probe requires a doubling of the number of wind-tunnel runs, in return for significant economy gains in probe calibration. This difficulty may be overcome by use of a three-dimensional computational scheme that properly treats the five-hole probe nose bluntness.

As described earlier, conventional use of five-hole conical probes requires an iterative data-processing procedure due to the variation of P_{av}/P_2 with θ. This variation is a combination of two effects. First, the local pitot pressure P_2 measured by a five-hole probe reduces slightly below that given by the Rayleigh pitot formula at large angles of attack. Figure 8 shows the variation of the ratio P_2/P_0 with θ reported by Centolanzi[11] at $M = 1.72$, 1.95, and 2.46, along with the current five-hole probe results at $M = 2.49$. Centolanzi[11] found that pitot pressure measurement using a conical probe was independent of both M and θ for $\theta \leq 25$ deg. Pitot pressure measurement using the current five-hole probe was found to be independent of θ for $\theta \leq 15$ deg. At $\theta = 25$ deg, P_2 was found to reduce by 2.3% below its value at $\theta = 0$ deg.

The second effect is the variation of P_{av} with θ. Previous investigators[11,13] have found that P_{av} increases with pitch angle, a fact that was confirmed in the five-hole probe measurements of the present study. However, both the four-hole probe results and computations performed for the current work showed no variation of P_{av} up to $\theta = 25$ deg at all Mach numbers included in the investigation. To illustrate this point, Fig. 9 shows a comparison of P_{av}/P_0 vs θ for the current five-hole, four-hole, and numerical results at $M = 2.49$. At $\theta = 25$ deg, the five-hole probe results show an increase in P_{av}/P_0 of 8.4% above the value at $\theta = 0$ deg. It is clear from this comparison that the variation of P_{av} with pitch angle is due to the nose bluntness. From the relative scale of these two competing effects it is clear that the variation of P_{av} with θ is the major cause for the iterative data-processing procedure required for five-hole probe measurements. As this effect has been found to be negligible for the four-hole probe, iteration need only be carried out in the current work to account for variation of P_2 with θ. For cone probe measurements

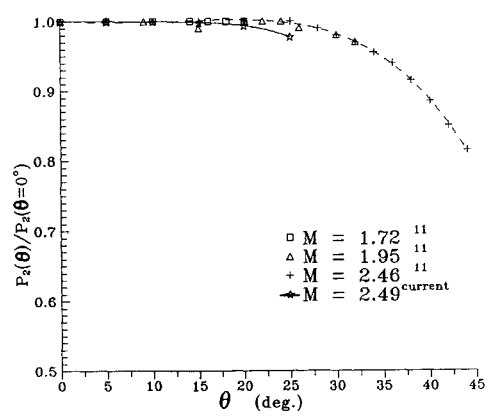

Fig. 8 Variation of pitot pressure with θ for 5-hole conical probes.

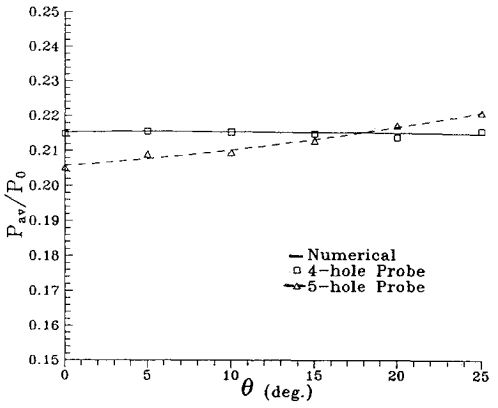

Fig. 9 Variation of average cone pressure with θ at M = 2.49.

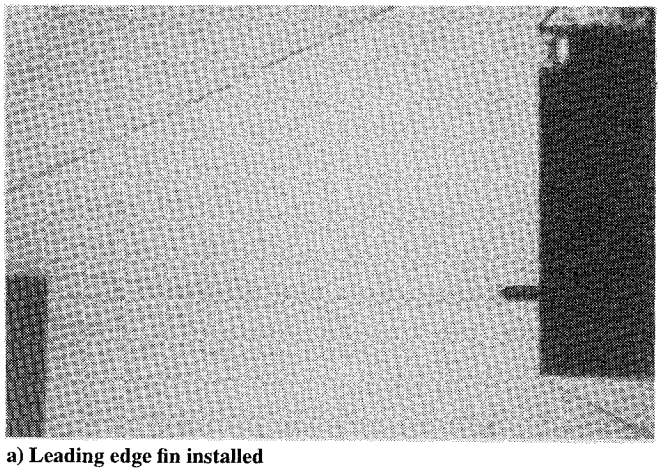

a) Leading edge fin installed

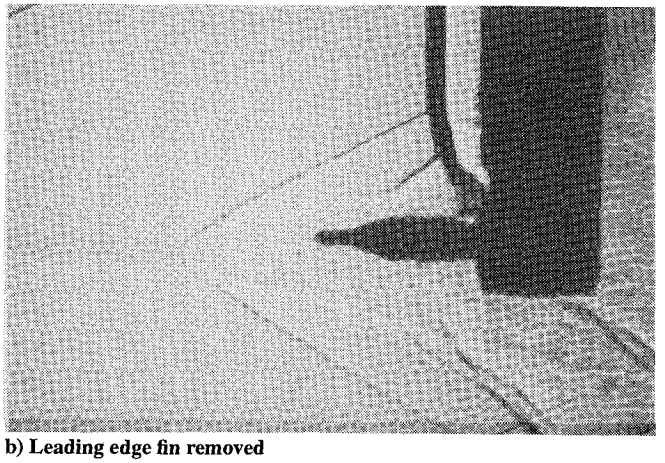

b) Leading edge fin removed

Fig. 10 Shadowgraphs of typical conical probe surveys of wing tip vortices at M = 2.49.

with $\theta \leq 15$ deg, variation of P_2 from that calculated using the Rayleigh pitot formula is assumed to be negligible in the current work, and hence data processing for these measurements reduced to a one-step procedure. For cone probe measurements with $\theta > 15$ deg, variation of P_2 with θ is accounted for using the curve generated by the current five-hole probe shown in Fig. 8, and data processing for these measurements required an iterative procedure, typically including one or two iterations.

Vortex Surveys

Conical probe surveys were conducted for the wing tip vortices generated by the half-wing at $\alpha = 5.7$ and 10.4 deg. In this work, the vortex generated by the half-wing at $\alpha = 5.7$ deg will be called the weak vortex, and that generated by the half-wing at $\alpha = 10.4$ deg will be called the strong vortex. A shadowgraph of the flow taken during a typical conical probe survey of the strong vortex is shown in Fig. 10a. Flow is from left to right, and the vortex core

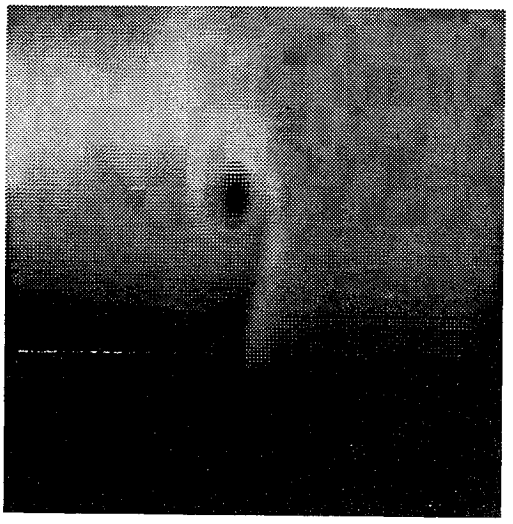

Fig. 11 Laser light sheet image of a wing tip vortex with α = 10.4 deg.

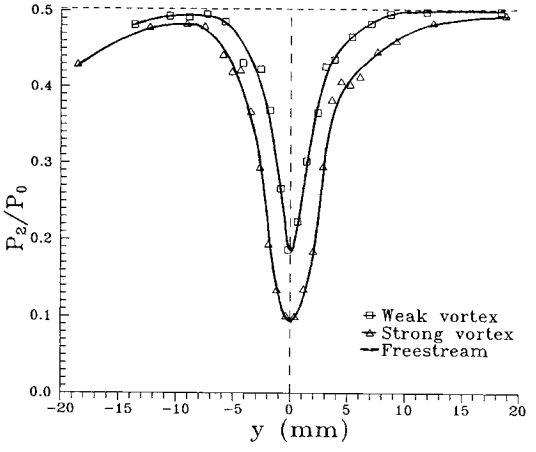

Fig. 12 Pitot pressure distribution in the vortex cores.

can be seen convecting downstream from the tip of the half-wing towards the conical probe. The shadowgraph clearly indicates that the probe is free of any support interference. Figure 10b shows a shadowgraph of the same flow but with the leading-edge fin removed from the probe support tube. Here the intersection of the vortex with the detached bow shock on the support tube generates the observed large-scale vortex distortion and renders the conical probe useless. Similar vortex distortions were reported in Ref. 1 for the head-on interaction of wing tip vortices with wedge leading edges. This figure vividly illustrates one of the difficulties that can be encountered during intrusive measurements of vortical flows. The vortex distortion was removed by addition of a leading-edge fin (18 deg included angle) that generates a significantly weaker shock than the support tube, while still supplying the required structural stability to the probe. An image of the $\alpha = 10.4$ deg tip vortex generated by a laser light sheet technique is shown in Fig. 11. The sheet was projected normal to the flow direction approximately 3 chords downstream of the half-wing (probe removed), and the view shown is looking downstream. The vortex core can be clearly seen in the image surrounded by an asymmetric swirling structure that joins up with the half-wing wake in the lower portion of the image.

The survey of each tip vortex was conducted 2.25 chords downstream of the half-wing trailing edge in a spanwise (vertical) line through the axis of each vortex. The position of the vortex axis is defined as the position at which the pitot pressure was observed to be a minimum. The downwash (Fig. 1) of each vortex is then the perpendicular distance from the streamwise plane through the centroid of the half-wing planform to the position of minimum pitot pressure. The downwash of the weak and strong vortices at the survey station was observed to be approximately 2.0 and 2.5 mm, respectively. The inwash (Fig. 1) of each vortex is the spanwise distance between the

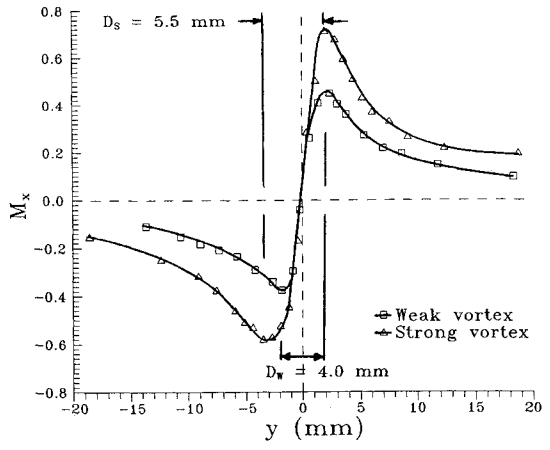

a) Swirl Mach number (M_x)

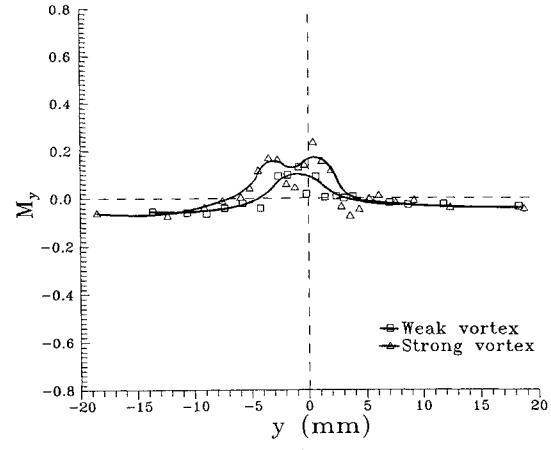

b) Spanwise Mach number (M_y)

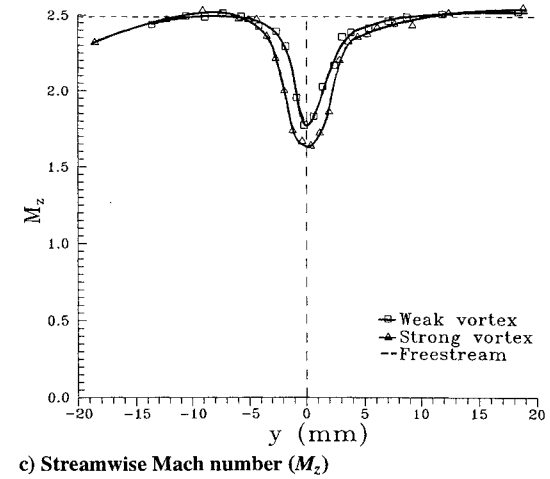

c) Streamwise Mach number (M_z)

Fig. 13 Mach number distributions in the vortex cores.

half-wing tip and the vortex axis. The inwash of the weak and strong vortices at the survey station was observed to be 3.4 and 4.3 mm, respectively. Having specified the position of the vortex axes at the survey station, all results of the vortex surveys are plotted with respect to a Cartesian coordinate system with origin at the respective vortex axes and the same orientation as the coordinate system used for the probe (Fig. 3).

The spanwise pitot pressure distributions for both the weak and strong tip vortices are shown in Fig. 12, indicating that the tip vortices are regions of significant pitot pressure deficit relative to the freestream. In particular, the pitot pressure distribution in the weak vortex dips to a minimum of $P_2/P_0 = 0.187$ and approaches the freestream value of $P_2/P_0 = 0.503$ approximately 9 mm outboard of the half-wing tip. Some effect of the wake may be seen at the inboard limit of the survey where the pitot pressure contin-

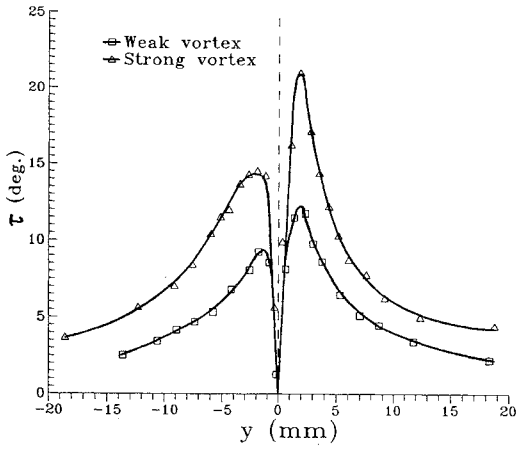

Fig. 14 Swirl angle distribution in the vortex cores.

ues to decrease after peaking just below the freestream value. For the strong vortex the pitot pressure is seen to reach a minimum of $P_2/P_0 = 0.101$ and approaches the freestream value 15 mm outboard of the half-wing tip. Some evidence of half-wing wake is also observed in a similar fashion to the weak vortex. In general, the magnitude and spatial scale of the pitot pressure deficit increases with half-wing angle of attack.

Figures 13a–13c show the Mach number distributions for both vortices. Since significant variation in the pitot pressure occurs over lengths of the order of the diametral distance between opposite surface pressure taps (2.0 mm), the pitot value used to calculate the flow properties was averaged over a 2.0-mm length centered on the conical probe tip. Figure 13a shows the distribution of the lateral component of Mach number (M_x) for both vortices. For the geometry of the current experiments, M_x may be interpreted as the swirl component of the Mach number. The distributions show a similarity to the classic Burgers' swirl velocity profile with an inner linear swirl distribution, surrounded by a region with swirl similar to an irrotational vortex. The point of zero swirl was found to correspond closely with the vortex axes. It is noted, however, that the profiles are not symmetric but show a larger swirl outboard of the half-wing (see also Fig. 11). This asymmetry is also typical of low-speed wing tip vortices.[5] The average core diameters of the weak and strong vortices (measured from peak to peak in the M_x distribution) were observed to be $D_w = 4.0$ mm and $D_s = 5.5$ mm, respectively.

Figure 13b shows the distribution of the spanwise component of Mach number (M_y) for both vortices. To interpret the observed M_y distributions, it is worth noting that these show the radial Mach number component in the vortex core in combination with the inwash of the tip vortex and the wake. The main conclusion obtained from these distributions is that both these effects are of significantly smaller magnitude than the vortex swirl. Figure 13c shows the distribution of the streamwise component of Mach number (M_z) for both vortices. Significant Mach number deficit is observed to occur for both vortices in a small region near their respective axes. Outside this region, which is of the same spatial scale as the vortex core, M_z was observed to be close to M_∞. The wake-like M_z profiles reach a minimum of $M_z = 1.77$ and 1.64 for the weak and strong vortices, respectively. The wake-like streamwise Mach number distributions observed here are similar to those found in low-speed wing tip vortices[5] and are attributed to the momentum deficit in the half-wing boundary layer. Streamwise Mach number deficits of this magnitude have important implications for vortex interaction studies.

Based on the results presented in Figs. 13a and 13c, the magnitude of the vortex swirl angle τ is plotted in Fig. 14. As noted earlier, the vortices are not axisymmetric, leading to a peak swirl angle outboard of the half-wing tip. The maximum swirl angles are $\tau = 11.8$ and 21.0 deg for the weak and strong vortices, respectively. The spanwise total pressure distributions for the weak and strong vortices are shown in Fig. 15. As expected, significant total pressure deficits occur in the core regions, the minimum total pressure being $P_1/P_0 = 0.21$ and 0.12 for the weak and strong vortices, respectively. Figure 16 shows the static pressure distribution in the

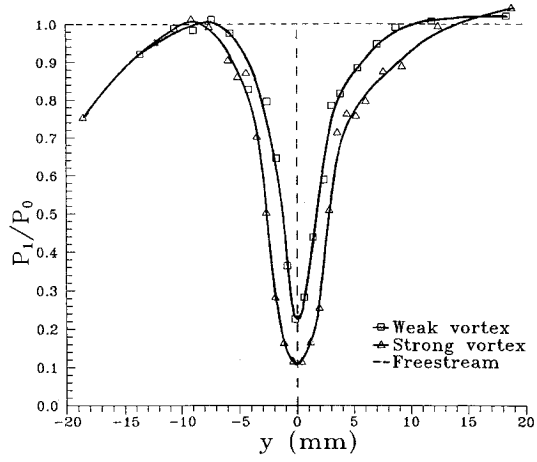

Fig. 15 Total pressure distribution in the vortex cores.

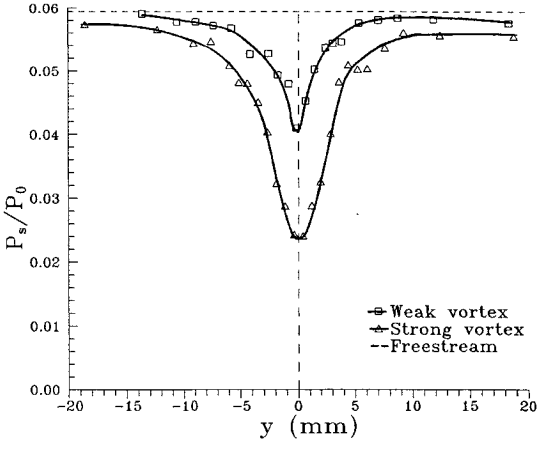

Fig. 16 Static pressure distribution in the vortex cores.

tip vortices. The static pressure can be seen to drop well below its freestream value of $P_s/P_0 = 0.059$ for both vortex strengths, reaching a minimum of $P_s/P_0 = 0.045$ and 0.024 for the weak and strong vortices, respectively. A noteworthy feature of the results is the absence of any effect of the shock-expansion wave structure generated by the half-wing. This indicates that the survey position 2.25 chords downstream of the half-wing trailing edge is within the "test diamond" for the current experiments. In summary, the supersonic wing tip vortices exhibited many characteristics commonly found in low-speed wing tip vortices, including an asymmetric Burger-like swirl distribution and significant total and static pressure deficits. The spatial scale, swirl, and pressure deficits of the vortices were observed to increase with half-wing angle of attack.

Conclusions

Conical probe surveys were conducted at Mach 2.49 for the wing tip vortices generated by a rectangular half-wing at 5.7 and 10.4 deg angle of attack. The tip vortices exhibited many characteristics similar to their low-speed counterparts, including asymmetric Burger-like swirl distributions and significant total and static pressure deficits. A wake-like streamwise Mach number distribution was observed for both tip vortices, and the size, swirl, and pressure deficits of the vortices increased with the half-wing angle of attack. These results add to the small amount of experimental supersonic tip vortex data available in the literature. Computational calibration of commercially available conical probes using a conical Euler solver was found to be satisfactory for pointed four-hole probes. Extension of numerical calibration to blunt five-hole conical probes would require a treatment of the nose bluntness in the numerical model, which was not attempted here. The current use of computational fluid dynamics to calibrate conical probes has been shown to be a viable alternative to conventional experimental calibration, particularly when wind-tunnel time is at a premium.

Acknowledgments

This work was supported by the Air Force Office of Scientific Research under Grant F49620-93-1-0009 and by NASA Lewis Research Center under Grant NAG3-1378. Computing resources were provided by the Pittsburgh Supercomputing Center. The authors are grateful to Frank Marconi for providing the computer code used to generate the calibration curves. The assistance of Lester Orlick, Kuo-Kuang Liu, and Joe Zammit was greatly appreciated during the work. Many useful discussions with Donald P. Rizzetta are acknowledged with appreciation.

References

[1]Kalkhoran, I. M., "Vortex Distortion During Vortex-Surface Interaction in a Mach 3 Stream," *AIAA Journal*, Vol. 32, No. 1, 1994, pp. 123–129.

[2]Kalkhoran, I. M., and Sforza, P. M., "Airfoil Pressure Measurements During Oblique Shock Wave-Vortex Interaction in a Mach 3 Stream," *AIAA Journal*, Vol. 32, No. 4, 1994, pp. 783–788.

[3]Smart, M. K., and Kalkhoran, I. M., "The Effect of Shock Strength on Oblique Shock-Wave/Vortex Interaction," AIAA Paper 95–0098, Jan. 1995.

[4]McCormick, B. W., Tangler, J. L., and Sherrieb, H. E., "Structure of Trailing Vortices," *Journal of Aircraft*, Vol. 5, No. 3, 1968, pp. 260–267.

[5]Orloff, K. L., "Trailing Vortex Wind Tunnel Diagnostics with a Laser Velocimeter," *AIAA Journal*, Vol. 11, No. 8, 1974, pp. 477–482.

[6]Corsiglia, V. R., Schwind, R. G., and Chiger, N. A., "Rapid Scanning, Three-Dimensional Hot Wire Anemometer Surveys of Wing Tip Vortices," *Journal of Aircraft*, Vol. 10, No. 12, 1973, p. 752.

[7]Baker, G. R., Barker, S. J., Bofah, K. K., and Saffman, P. G., "Laser Anemometer Measurements of Trailing Vortices in Water," *Journal of Fluid Mechanics*, Vol. 65, Pt. 2, 1974, pp. 325–336.

[8]Davis, T., "The Measurement of Downwash and Sidewash Behind a Rectangular Wing at Mach 1.6," *Journal of Aeronautical Science*, Vol. 19, No. 5, 1952, p. 329.

[9]Adamson, D., and Boatright, W. B., "Investigation of Downwash, Sidewash and Mach Number Distribution Behind a Rectangular Wing at Mach 2.41," NACA TR 1340, July 1950.

[10]Wang, F. Y., and Sforza, P. M., "An Experimental Investigation of Tip Vortices at Mach 2.5," AIAA Paper 93-3448, Aug. 1993.

[11]Centolanzi, F. J., "Characteristics of a 40 deg Cone for Measuring Mach Number, Total Pressure and Flow Angles a Supersonic Speeds," NACA-TN-3967, May 1957.

[12]Andrews, D. R., and Sawyer, W. G., "The Calibration of a 60 deg Cone to Measure Mach Number, Total Pressure, and Flow Angles at Supersonic Speeds," Aeronautical Research Council, CP-628, London, June 1962.

[13]Naughton, J. W., Cattafesta, L. N., and Settles, G. S., "Miniature, Fast-Response 5-Hole Conical Probe for Supersonic Flowfield Measurement," *AIAA Journal*, Vol. 31, No. 3, 1993, pp. 453–458.

[14]Oberkampf, W. L., and Aeschliman, D. P., "Joint Computational/Experimental Aerodynamics Research on a Hypersonic Vehicle, Part 1: Experimental Results," *AIAA Journal*, Vol. 30, No. 8, 1992, pp. 2000–2009.

[15]McWherter Walker, M., and Oberkampf, W. L., "Joint Computational/Experimental Aerodynamics Research on a Hypersonic Vehicle, Part 2: Computational Results," *AIAA Journal*, Vol. 30, No. 8, 1992, pp. 2010–2016.

[16]Peake, D. J., Fischer, D. F., and McRae, D. S., "Flight, Windtunnel and Numerical Experiments with a Slender Cone at Incidence," *AIAA Journal*, Vol. 20, No. 10, 1982, pp. 1338–1345.

[17]Kalkhoran, I. M., Cresci, R. J., and Sforza, P. M., "Development of Polytechnic University's Supersonic Wind Tunnel Facility," AIAA Paper 93-0798, Jan. 1993.

[18]Marconi, F., private communication, Grumman Corporate Research Center, Bethpage, NY, 1993.

[19]Beam, R. M., and Warming, R. F., "An Implicit Factored Scheme for the Compressible Navier–Stokes Equations," *AIAA Journal*, Vol. 16, No. 4, 1978, pp. 393–402.

[20]Roe, P. L., "Discrete Models for the Numerical Analysis of Time-Dependent Multidimensional Gas Dynamics," *Journal of Computational Physics*, Vol. 63, No. 2, 1986, pp. 458–476.

[21]Thomas, J. L., and Walters, R. W., "Upwind Relaxation Algorithms for the Navier–Stokes Equations," *AIAA Journal*, Vol. 25, No. 4, 1987, pp. 527–534.

[22]Rainbird, W. J., "The External Flow About Yawed Circular Cones," *Hypersonic Boundary Layers and Flow Fields*, AGARD-CP-30, May 1968, pp. 19-1–19-10.

[23]Feldhuhn, R. H., Winkelmann, A. E., and Pasiuk, L., "An Experimental Investigation of the Flowfield Around a Yawed Cone," *AIAA Journal*, Vol. 9, No. 6, 1971, pp. 1074–1081.

[24]Krasnov, N. F., *Aerodynamics of Bodies of Revolution*, Elsevier, New York, 1970.